

On the influence of stator-rotor radial gap size on the fluid-dynamic performance of mini-orc supersonic turbines

Cappiello, Alessandro; Majer, Matteo; Tuccillo, Raffaele; Pini, Matteo

DOI

[10.1115/GT2022-83309](https://doi.org/10.1115/GT2022-83309)

Publication date

2022

Document Version

Final published version

Published in

Turbomachinery - Axial Flow Turbine Aerodynamics; Deposition, Erosion, Fouling, and Icing; Radial Turbomachinery Aerodynamics

Citation (APA)

Cappiello, A., Majer, M., Tuccillo, R., & Pini, M. (2022). On the influence of stator-rotor radial gap size on the fluid-dynamic performance of mini-orc supersonic turbines. In *Turbomachinery - Axial Flow Turbine Aerodynamics; Deposition, Erosion, Fouling, and Icing; Radial Turbomachinery Aerodynamics* Article V10BT35A015 (Proceedings of the ASME Turbo Expo; Vol. 10-B). The American Society of Mechanical Engineers (ASME). <https://doi.org/10.1115/GT2022-83309>

Important note

To cite this publication, please use the final published version (if applicable). Please check the document version above.

Copyright

Other than for strictly personal use, it is not permitted to download, forward or distribute the text or part of it, without the consent of the author(s) and/or copyright holder(s), unless the work is under an open content license such as Creative Commons.

Takedown policy

Please contact us and provide details if you believe this document breaches copyrights. We will remove access to the work immediately and investigate your claim.

Green Open Access added to TU Delft Institutional Repository

'You share, we take care!' - Taverne project

<https://www.openaccess.nl/en/you-share-we-take-care>

Otherwise as indicated in the copyright section: the publisher is the copyright holder of this work and the author uses the Dutch legislation to make this work public.

GT2022-83309

**ON THE INFLUENCE OF STATOR-ROTOR RADIAL GAP SIZE ON THE
FLUID-DYNAMIC PERFORMANCE OF MINI-ORC SUPERSONIC TURBINES**

Alessandro Cappiello

Department of Industrial Engineering
"Federico II" University of Naples
80125 Naples, Italy
Email: alessandro.cappiello@unina.it

Matteo Majer

Department of Propulsion and Power
Faculty of Aerospace Engineering
Technical University Delft
Kluyverweg 1, 2629 HS, Delft, The Netherlands
Email: m.majer@tudelft.nl

Raffaele Tuccillo

Department of Industrial Engineering
"Federico II" University of Naples
80125 Naples, Italy
Email: raffaele.tuccillo@unina.it

Matteo Pini*

Department of Propulsion and Power
Faculty of Aerospace Engineering
Technical University Delft
Kluyverweg 1, 2629 HS, Delft, The Netherlands
Email: m.pini@tudelft.nl

ABSTRACT

Radial-Inflow Turbines are considered the most suited expanders for waste heat recovery via high-temperature mini-organic Rankine Cycle (ORC) turbogenerators thanks to high compactness, large expansion ratio handled by a single stage, and comparatively low weight. Reaching high efficiency in these machines is however a formidable challenge, as they are bounded to operate with expansion ratios exceeding 40.

Although scarcely investigated in the published literature, the size of the stator-rotor radial gap is a key design parameter as it has a large influence on fluid-dynamic performance, manufacturing, and mechanical integrity. In addition, the working conditions of the turbine are such that the stator operates with highly supersonic flows in the non-ideal thermodynamic regime, making the flow pattern in stator-rotor radial gap, which can be regarded as an area-decreasing channel, very complex. Under these conditions, the radial gap size could impact the stage efficiency

up to few percentage points. The paper presents a study aimed at investigating the impact of variable radial gap on the fluid-dynamic performance of radial-inflow turbines for high-temperature mini-ORC power systems. The reference turbine is a supersonic machine for laboratory experiments under realization at Delft University of Technology, referred to as ORCHID turbine. First, a theoretical analysis is carried out to identify the relevant non-dimensional parameters governing the flow physics in the gap. Then, the effect of the radial gap size on the fluid-dynamic performance of the ORCHID turbine is assessed by means of RANS and uRANS computations. The results show that the change in radial gap size leads to a redistribution of expansion ratio between vaned and vaneless part of stationary component via a substantial change of the stator trailing edge flow structures, which, in turn strongly affects stator loss and stage efficiency, leading to 8% points reduction.

*Address all correspondence to this author.

NOMENCLATURE

a	Speed of Sound
A	Area
b	Channel Height
c	Vane or Blade Chord
g	Pitch
h	Average mesh spacing
Ma	Mach Number
p	Pressure
R	Radius
Re	Reynolds Number
T	Temperature
s	Entropy
w	Thickness
Z	Vane or Blade Count

Greek Symbols

Ω	Rotational Speed
α	Absolute flow angle
β	Relative flow angle
ρ	Density
σ	Solidity
Π	Expansion ratio

Subscripts

In	Inlet
Ise	Iisentropic
h	Hub
met	Metal Angle
N	Nozzle
Out	Outlet
R	Rotor
s	Shroud
t	Total Quantity
tg	Target
th	Inner Throat
0	Stator inlet
1	Stator outlet
2	Rotor inlet
3	Rotor outlet

Acronyms

CFD	Computational Fluid-Dynamics
LE	Leading Edge
LR	Left-Running
LuT	Look-up Table
MOC	Method of Characteristics
ORC	Organic Rankine Cycle
PS	Pressure Side
RANS	Reynolds-Averaged Navier–Stokes

RIT	Radial-Inflow Turbine
RR	Right-Running
SS	Suction Side
TE	Trailing Edge

INTRODUCTION

High-Temperature Organic Rankine Cycle (ORC) systems are considered a key technology for the reduction of CO₂ emissions from prime movers and power plants Ref. [1,2]. A sector in which this technology might find future application is aviation. The potential of Waste Heat Recovery in aviation is theoretically large, given that about 50% of the input chemical energy is discharged in the form of hot, high speed gas flow, from the main engines and from gas turbines used to generate on-board electric power. Recovering just a fraction of this untapped energy by means of ORC systems might provide substantial advantage in terms of reduction of fuel consumption. However, this is a formidable challenge as the improvement in thermodynamic efficiency of the engines has to outweigh the penalty introduced by the weight of the WHR system.

The Propulsion and Power group of Delft University of Technology is investigating the use of lightweight high-temperature ORC systems for airborne waste heat recovery, Ref. [3], in which the turbo-expander is constituted by a single-stage supersonic turbine. A radial-inflow turbine (RIT) (Ref. [4]) featuring a total-static pressure ratio of 41, a maximum absolute Mach number of about 2 and a calculated power of ~ 11 kW has been chosen for the realization of an experimental test rig. Apart from the measurement of the overall turbine performance, the rig should also provide access to direct flow measurements in the radial gap between the stator and the rotor.

The size of the radial gap is one of the most relevant parameter affecting turbine performance. On the one hand, a larger radial gap induces lower aero-mechanical interaction, but higher mixing losses. On the other hand, a small gap limits viscous loss and leads to a more compact assembly, but at the expense of a decrease of flow uniformity upstream of the rotor. To date, very few authors investigated the effect of the radial gap size on stage performance. In the 1960s, A. P. Tunakov was the first, to the author's knowledge, who extensively studied the radial gap in RITs, Ref. [5]. Intuitively, he concluded that an excessively small radial gap can cause an efficiency penalty due to poor flow uniformity at the rotor inlet, while a large efficiency penalty due to friction losses arises when using large radial gaps. Tunakov devised a rule to capture this trade-off in the preliminary design:

$$\frac{\Delta R}{b \cdot \sin(\alpha)} \cong 2 \quad (1)$$

According to Eqn. (1), the optimal radial gap size ΔR is proportional to the gap height b and the stator discharge flow angle α . In 1971, Watanabe et al., Ref. [6], performed experiments on a radial-axial turbine selecting a set of vanes to yield constant exit flow velocities and equal flow angles. The authors observed that increasing the radial gap leads to an increase in reaction degree, and viceversa. Furthermore, they found the gap size to have a relatively low impact on the efficiency, as they varied the radial gap ratio R_1/R_2 from 1.05 to 1.25.

Other authors investigated the impact of varying the radial gap on turbine performance. In Ref. [7], the authors documented an analytical method to evaluate the viscous loss in the radial gap. In the range of operating conditions and flow regimes investigated, the loss was found to be slightly influenced by the stator discharge Mach number. More recently, Simpson et al., Ref. [8], investigated the stage performance of a radial-inflow turbine operating with low temperature air. They manufactured and tested a series of stator rings varying the radial gap size at constant blade count. They found that the efficiency penalty when varying the radial gap is negligible.

When a small scale radial turbine for high-temperature ORC systems is considered, the findings from previous works may not be applicable. The very large pressure ratio typical these machines leads to highly supersonic stator discharge, with Mach number exceeding 2, Ref. [9, 10]. In addition, the use of fluids made by complex molecules and exhibiting non-ideal gas-dynamic behaviour Ref. [11, 12] has a large influence on turbine fluid-dynamic performance, Ref. [13, 14], as well as on flow pattern downstream of the stator trailing edge, Ref. [15, 16, 17]. Consequently, the flow uniformity at rotor inlet results greatly affected, see Ref. [18, 19], and particularly critical for aspects related to aero-forcing, Ref. [20], power output fluctuations, and fluid-dynamic losses, Ref. [21].

In this paper, the impact of the radial gap on the fluid-dynamic performance of a mini-ORC RIT has been investigated. The goal of this study is twofold: 1) to broaden the understanding of the flow physics in the vaneless region of the stator-rotor radial gap of supersonic, mini radial-inflow turbines 2) to infer on the choice of radial gap size that yields the maximum aerodynamic performance.

METHODOLOGY

Theoretical Considerations

A simplified analysis is used to assess the impact of the radial gap size on turbine degree of reaction. Assuming that the flow angle in the vaneless region is unaffected by the change of radius, the critical area ratio for a perfect gas can be conveniently defined between the stator vane throat and the rotor inlet section as:

$$\frac{A_2}{A_{th}} = \frac{1}{Ma_2} \cdot \left[\frac{2 + (\gamma - 1) \cdot Ma_2^2}{\gamma + 1} \right]^{\frac{\gamma + 1}{2(\gamma - 1)}} \quad (2)$$

Because the area ratio on the left-hand side of Eqn. (2) is fixed by the mass-flow rate of the turbine and by the rotor entry area, the rotor inlet *Mach* number Ma_2 is unequivocally defined to satisfy Eqn. (2).

Assuming that the total pressure losses upstream of the rotor are negligible, the *total-static pressure ratio* across the stage can be expressed as:

$$\beta_{ts} = \frac{P_{t0}}{P_3} \cong \frac{P_{t2}}{P_3} = \frac{P_2}{P_3} \cdot \frac{P_{t2}}{P_2} \quad (3)$$

It then follows that the ratio between total and static pressure at rotor inlet, P_{t2}/P_2 , is fixed by the *Mach number* Ma_2 for the well-known stagnation relation. As a result, a given stage pressure ratio, β_{ts} , thus fixes the rotor static-static pressure ratio P_2/P_3 . This, in turn, leads to the result: $P_2 = constant$.

When changing the radial gap, being the rotor design and the design mass flow rate fixed, the overall area ratio, A_{th}/A_2 , is unchanged. However, as the latter can be expressed as in Eqn. 4, one can see that a radial gap change entails a different split of the overall area ratio over the stationary part.

$$\frac{A_{th}}{A_2} = \frac{A_{th}}{A_1} \cdot \frac{A_1}{A_2} \quad (4)$$

In conclusion, it is reasonable to expect that a radial gap variation yields only a redistribution of the expansion ratio across the stator vanes and the vaneless space, while keeping the overall expansion ratio and the degree of reaction fixed.

Aerodynamic Shape Design

The turbine designed and documented in Ref. [4] has been used to investigate the radial gap influence on performance of supersonic RITs. In fact, the latter device is representative of very high pressure ratio, highly supersonic radial turbines for mobile ORC applications. A scheme of the turbine configuration, highlighting the main stations along the flow-path, has been provided in Fig. 1.

Following the approach proposed by the authors of Ref. [6, 8], the radial gap, whose extension will be hereon conveniently referred to by means of the radius ratio R_1/R_2 , has been varied as summarized in Tab. 1. The nozzle outlet Mach number, Ma_{tg} , and the associated metal angle, α_{met} , which resulted from the original design optimisation performed by Ref. [4], have been kept fixed to isolate the influence of the radius ratio R_1/R_2 . As a side note, the value of the nozzle target Mach number, has been slightly adjusted with respect to that of Ref. [4], to operate with a minimum amount of post-expansion at design conditions and improve the off-design behavior of the machine. Nevertheless, the off-design performance is not part of the present work and will therefore not be discussed.

Stator Geometry A manufacturing feasibility study by TU Delft's in-house workshop has been conducted on the original stator vane from Ref. [4], which led to increasing the

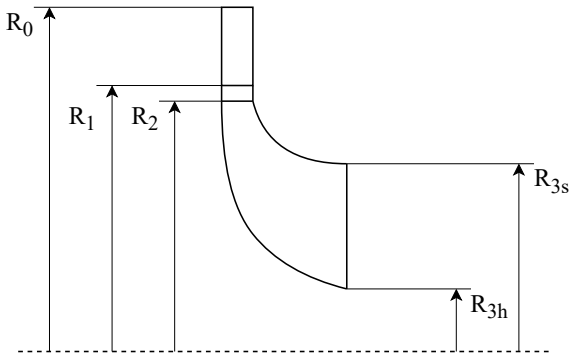


FIGURE 1: SCHEME OF THE INVESTIGATED RADIAL-INFLOW TURBINE HIGHLIGHTING THE MAIN STATIONS ALONG THE FLOW PATH — THE FLOW ENTERS RADIALLY INWARD FROM 0 AND LEAVES THE TURBINE AXIALLY AT STATION 3

stator trailing edge thickness from < 0.1 mm up to ≥ 0.2 mm. This resulted in more than doubling the trailing edge thickness to pitch ratio with respect to the original design, since the pitch was kept constant to maintain the cascade solidity nearly unchanged (see Tab. 1)¹.

A set of radial vane cascades was then designed for increasing radial gap ratio, keeping nearly constant Reynolds number based on the chord and isentropic, divergent exit section properties. The TE thickness has been adapted for each case to ensure similar thickness to pitch ratio among the set of geometries compared. The maximum solidity deviation remained within -1.5% with respect to the baseline geometry, which ensures limited impact of cascade solidity on the results. Furthermore, it is worth mentioning that the geometry $\Delta R4$ has been sized according to Tunakov's rule, as per Eqn. 1.

The stator vanes investigated in the present work have been designed by means of an in-house code based on the Method of Characteristics (MOC). The tool can perform the design of axial and radial-inflow converging-diverging cascades for either ideal and non-ideal flows (see *OpenMOC* code, Ref. [10, 22]). To carry out the study hereby presented, the code was modified and the following operations were performed within the code:

1. Determine the non-dimensional geometry of the divergent nozzle by solving the MOC to yield a target Mach number, Ma_{tg} , achieved at the divergent exit section.
2. Scale the core of the divergent section according to Eqn. 5, to deliver the design mass flow rate, \dot{m} , assuming the average Mach number at the geometric throat, A_{th} , equal to unity. The latter consideration is obviously not rigorously correct, but the discrepancy was deemed negligible after comparison with CFD results.
3. Insert the trailing edge (TE) as a semi-circle, of diameter equal to the desired thickness, set to be tangent to the stator outlet radius, R_1 , and oriented to yield a specific outlet metal angle, $\alpha_{met, Out}$.
4. Shift and rotate the nozzle core (obtained at point 2) to achieve tangency at the TE.
5. Rotate the nozzle core section tangent to the TE, together with the TE, by an angular pitch to obtain the supersonic portion of the pressure side (PS).
6. Draw a single NURBS curve to define the PS and suction side (SS) portions of the subsonic part of the vane,

$$A_{th} = \frac{\dot{m}}{Z_N b \rho_{th} a_{th}} \quad (5)$$

¹Stator and rotor geometries are available for download at: https://github.com/mmajerTUD/Metadata/tree/main/ORCHIDTurbine/ASME_TurboExpo_2022

minding the tangency of NURBS curve and convergent-divergent shape at the throat, A_{th} , to insure the continuity of the first derivative.

7. Finally, interpolate between the divergent exit section and the TE on the rear SS part to close the vane shape, once again by means of NURBS curve.

Such a procedure leads to a close, un-tapered and un-twisted vane profile that is subsequently meshed.

Rotor Geometry The rotor blade geometry of Ref. [4] was slightly modified to satisfy manufacturing constraints associated with a 5-axes milling process by TU Delft’s in-house manufacturing workshop. In particular, the blade thickness has been increased to achieve better geometrical tolerances while the blade count was reduced to allow the necessary space for the tool head during the cutting process. Tab. 2 provides an overview of the changes.

CFD Analysis

To assess the performance of the geometries studied in the present work, CFD calculations have been employed. Therefore, meshes of the computational domains have been built in ANSYS TurboGrid, setting $y^+ = 1$ along the vane and blade surfaces and $y^+ = 5$ at hub and shroud surfaces. Also, it is worth mentioning that the tip gap region was included in the computational domain to mesh.

Given the extremely close similarity of working conditions, say working fluid, stator and rotor chords, Reynolds

and Mach numbers, as well as rotational speed, all meshes used in the present work have been built with a cell count chosen so as to provide the same average mesh spacing, h Eqn. 6, used in Ref. [4], whose results were already proven to be mesh independent. Table 4 provides a summary of the main features of the mesh used for stator and rotor geometries.

$$h = \sqrt[3]{\frac{\text{Computational Domain Volume}}{\text{Cells Count}}} \quad (6)$$

The working fluid used throughout the work is siloxane MM and its properties have been described by means of Look-up Table (LuT) approach, with table size 1000x1000.

Concerning the computational methods, all calculations have been carried out in ANSYS CFX, employing different fidelity models. Particularly, 3D CFD steady-state RANS calculations have been performed on all geometries both for isolated stator cascades and complete stages. Instead, 3D unsteady RANS calculations of the complete stage have been performed for *Baseline*, ΔR_3 , ΔR_4 and ΔR_5 cases, so as to assess the reliability of steady-state stage results.

It is worth pointing out that in the case of steady-state stage calculations a mixing-plane was set at the stator-rotor interface – at $R \approx 1.01 \cdot R_2$ – to account for frame change; whereas for stator alone calculations, the computational domains have been enlarged downstream up to a radius $R \approx 0.90 \cdot R_2$.

The boundary conditions have been provided in terms of inlet total pressure, p_{t0} , and temperature, T_{t0} , together with outlet static pressure, p_3 , according to the values reported in Tab. 3 with the only exception of stator alone calculations, for which the outlet static pressure has been set to a different value, as explained in the forthcoming. In fact, in the latter the outlet static pressure was set to approximately match the static pressure found at the mixing plane of the corresponding baseline stage calculation, leading to an expansion ratio of the baseline stator computational domain of about 26.3. The expansion ratios for the stators with increased radial gaps were set to approximately the same value. This approach allowed to isolate the effect of the radial gap size on the fluid-dynamic performance of the stationary part.

All walls have been set to adiabatic with no-slip condition and $k-\omega$ SST turbulence model was used for turbulence closure. Finally, all simulation results have been obtained using 2nd order advection and high resolution turbulence schemes. Unsteady calculations featured a 1st order Backward Euler scheme adopting 100 time-steps for each rotor passing period.

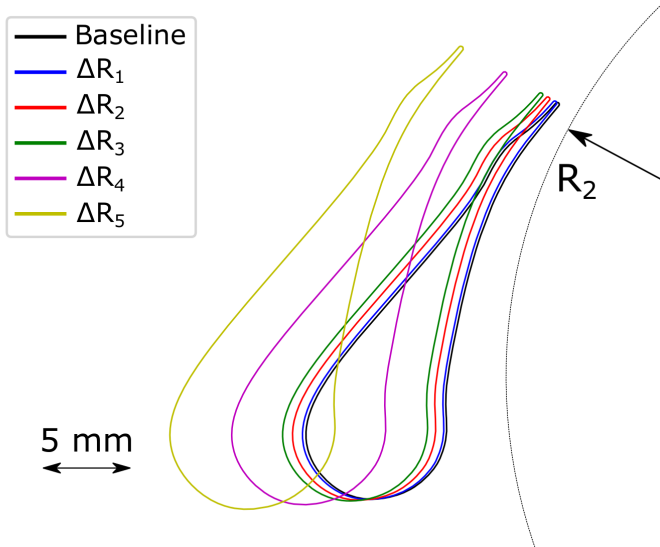


FIGURE 2: INVESTIGATED STATOR GEOMETRIES

TABLE 1: STATOR DESIGN VARIABLES

Case	Z_N	$\alpha_{met,1}$	Ma_{tg}	$\frac{w_{TE}}{g}$	$\frac{R_1}{R_2}$	σ	Re_c
-	-	deg	-	-	-	-	-
Original [4]	12	80	2	0.0054	1.037	1.51	$4 \cdot 10^6$
Baseline	12	80	1.91	0.0143	1.037	1.57	$4.14 \cdot 10^6$
$\Delta R1$	12	80	1.91	0.0143	1.043	1.56	$4.16 \cdot 10^6$
$\Delta R2$	12	80	1.91	0.0143	1.058	1.56	$4.2 \cdot 10^6$
$\Delta R3$	12	80	1.91	0.0143	1.074	1.56	$4.26 \cdot 10^6$
$\Delta R4$	12	80	1.91	0.0143	1.153	1.54	$4.51 \cdot 10^6$
$\Delta R5$	12	80	1.91	0.0143	1.250	1.51	$4.82 \cdot 10^6$

TABLE 2: ROTOR GEOMETRY

Case	Z_R	w_h	w_s	R_2
-	-	mm	mm	mm
Original [4]	19	0.37	0.17	25.75
New	16	0.6	0.3	25.75

TABLE 3: BOUNDARY CONDITIONS FOR STAGE CFD CALCULATIONS

Working Fluid	p_{t0}	T_{t0}	p_3	Ω
-	bar	K	bar	kRPM
MM	18.1	573	0.443	98.1

As convergence criteria for the stator alone calculations the residuals order of magnitude 10^{-7} was considered, while 10^{-5} was adopted for stage calculations, both steady and unsteady. In the latter case, maximum 7 iterations per time-step were used and a number of rotor passing periods large enough to achieve time-periodic convergence of monitored quantities, e.g., Mach number, at several locations was adopted.

RESULTS

Stator Analysis

The effect of a stator-rotor radial gap change on RIT convergent-divergent stators was investigated by performing CFD calculations on the six stator rows previously intro-

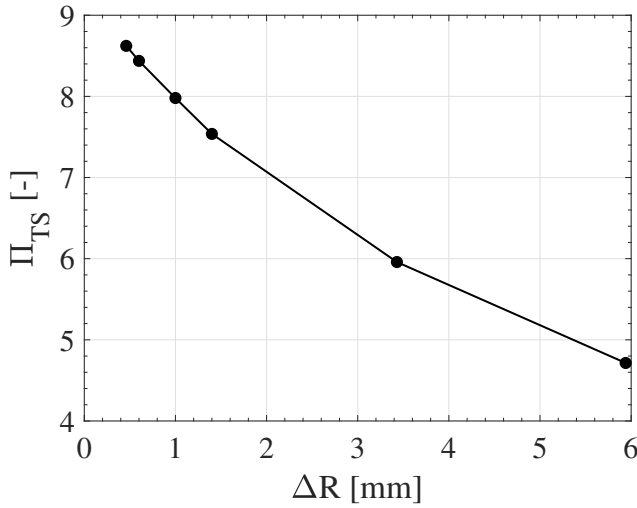
duced, and designed according to the values reported in Tab. 1, while keeping the expansion ratio fixed, as described in CFD Analysis section, to isolate the effect of the radial gap.

The global effects of the radial gap change are shown in Fig. 3a and 3b, presenting the total-static expansion ratio, p_{t0}/p_1 , and the thermodynamic efficiency, Eqn. (7). The latter has been calculated at both the stator TE and the mixing plane radii, in an attempt to isolate the gap's contribution to the overall loss.

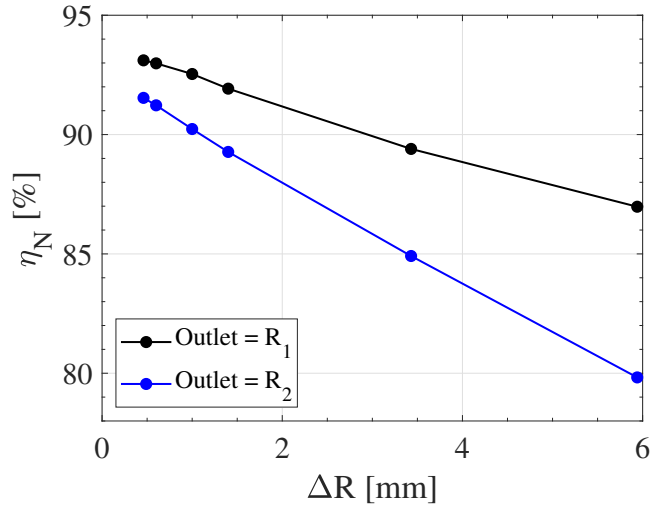
As one can see in 3a, a change in radial gap size yields a redistribution of the overall expansion ratio between stator and radial gap domains. Particularly, the stator share of the overall expansion ratio decreases as the radial gap increases, although this occurs with a non-negligible stator performance change, which worsens for increasing sizes of the radial gap, Fig. 3b. Interestingly, despite both curves in

TABLE 4: STATOR AND ROTOR MESH DATA

Cascade	Case	h	$\#_{cell}$
-	-	m	-
Rotor	New	$7.3 e^{-5}$	$1.65 e^6$
Stator	Baseline	$4.83 e^{-5}$	$2.11 e^6$
""	$\Delta R1$	$4.83 e^{-5}$	$2.14 e^6$
""	$\Delta R2$	$4.83 e^{-5}$	$2.3 e^6$
""	$\Delta R3$	$4.83 e^{-5}$	$2.42 e^6$
""	$\Delta R4$	$4.83 e^{-5}$	$3.23 e^6$
""	$\Delta R5$	$4.83 e^{-5}$	$4.22 e^6$



(a) STATOR TOTAL-TO-STATIC EXPANSION RATIO



(b) STATOR EFFICIENCY

FIGURE 3: EFFECT OF RADIAL GAP SIZE CHANGE OVER STATOR PERFORMANCE

Fig. 3b show the same trend, the stator efficiency penalty appears to be much larger if the radial gap domain is included in the efficiency computation, highlighting a substantial loss contribution taking place in the radial gap.

$$\eta_N = \frac{h_{t,In} - h_{Out}}{h_{t,In} - h_{Ise,Out}} \cdot 100 \quad (7)$$

To explain the trends of the expansion ratio redistribution and stator efficiency decrease occurring as the radial gap size is changed, its effect on the flow field should be thoroughly analyzed and understood. To this aim, Fig. 4 and 5 show the mid-span Mach number and pressure gradient, respectively, for the six stators investigated.

In Fig. 4 all the characteristic features of RIT supersonic vanes appear clearly and in a rather similar manner, e.g., the rapid expansion occurring in the throat region together with the Trailing Edge pattern, made up of expansion fans and shock waves. Conversely, a rather different stator wake dynamic stands out as a result of the radial gap size change. First of all, as the radial gap increases the stator wake travels in the domain longer; whereas, for low radial gap cases the wake is convected towards the domain exit faster. Secondly, as the radial gap increases, also the mixing process of the wake seems to be slower. In fact, for low radial gap cases by the time the wake crosses the reflected shock of the right-running TE pattern branch, it already appears well mixed. Conversely, for large radial gap size several wakes can be seen to cross the stator TE shocks. As a result, if a single

passage is considered, the larger the radial gap size the more wakes can be seen crossing the domain.

Nonetheless, a change in radial gap size strongly impacts the circumferential distributions of flow properties and wake profile found at rotor inlet radius. This occurrence is shown in Fig. 6, which presents the entropy pitch-wise distributions, together with their average values, found at rotor inlet radius for three out of six geometries. For the baseline case the wake profile can be clearly seen as a high entropy peak at about 0.15-0.4 pitch fraction, while the entropy increase due to the stator TE shocks can be seen as two small cusps in the distributions. The wake footprint on the entropy pitch-wise distributions is instead considerably wider for the ΔR_3 case, 0.6-1.0 pitch fraction. Finally, if the ΔR_5 case is considered, the wake profile is rather difficult to identify, as almost the whole pitch is affected by the stator TE wake. This occurrence can be easily explained considering that, while the flow travels downstream, further away from the vane TE, the stator TE wake mixing process advances, leading the entropy to increase and, at the same time, the wake profile to enlarge. When the radial gap size is increased, at rotor inlet radius the flow has travelled a longer distance from the stator TE. Therefore, the wake mixing is at a more advanced stage. This is also witnessed by the larger average values of entropy found at rotor inlet radius as the radial gap increases, Fig. 6.

The mid-span pressure gradient contours shown in Fig. 5 with the superposition of the streamlines allows the assessment of the effect of a radial gap change on the TE pattern, that is in fact the main driver of the expansion ra-

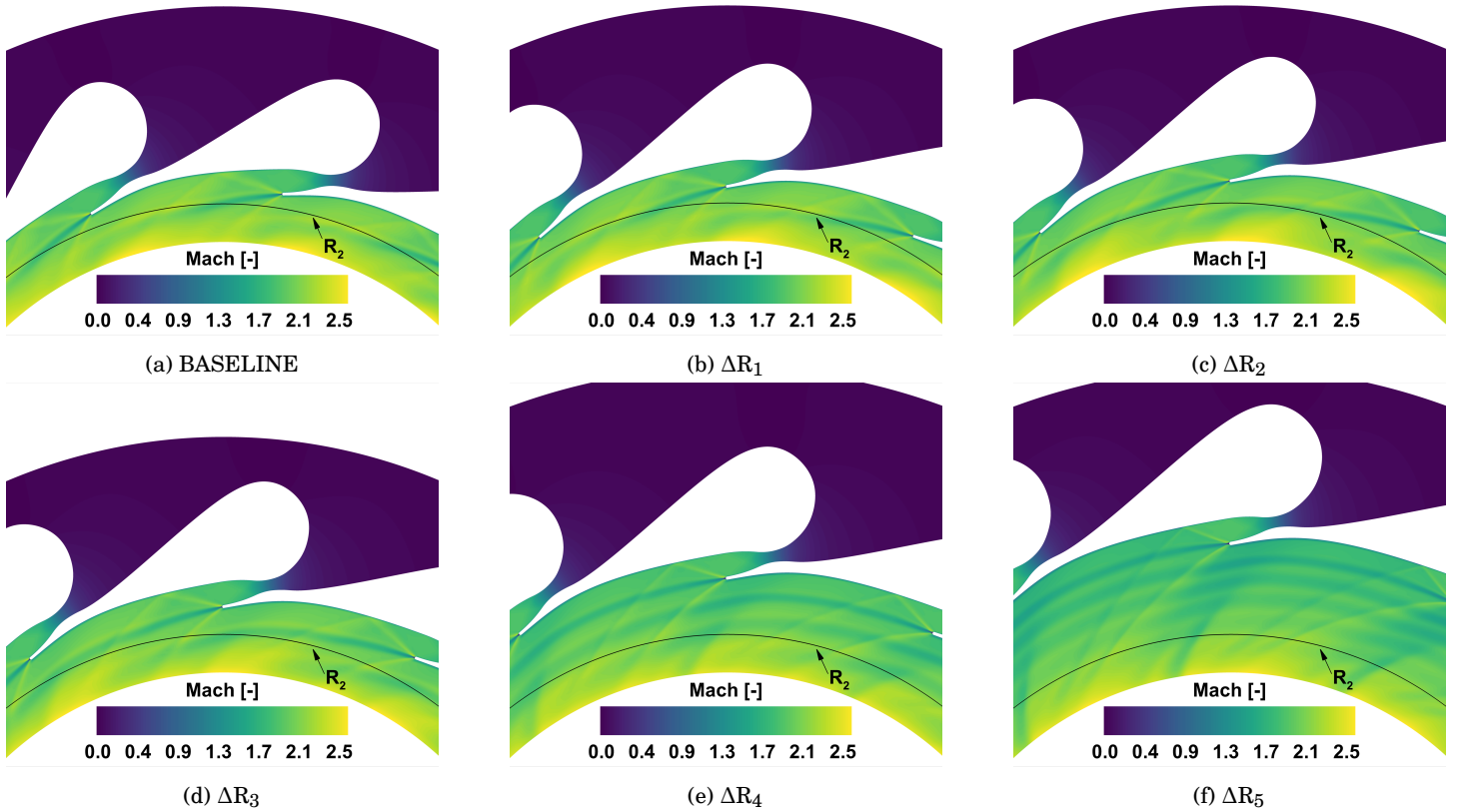


FIGURE 4: MID-SPAN MACH NUMBER CONTOURS.

tion redistribution seen in Fig. 3a. Particularly, increasing the radial gap several changes can be noticed in Fig. 5: on the one hand, the Right-Running (RR) expansion fan **A** at the TE shrinks and, therefore, reduces the post expansion and in turn the expansion ratio achieved upstream of the surface tangent to the stator TE (subscript 1), which forces the right-running shock **B** to move upstream. Also, it is evident that the RR TE shock progressively intensifies from the baseline case of Fig. 5a to the ΔR_5 case of Fig. 5f, affecting the stator vanes blade loading.

This occurrence is shown in Fig. 7, where the impinging expansion fan and shock wave – generated by the adjacent vane TE – determines a progressively higher unloading as the radial gap was increased, which starts at about 0.85 of the stream-wise coordinate. Therefore, the loss increase seen in Fig. 3a upstream of the trailing edge can arguably be ascribed to stronger shocks impinging on the adjacent vane SS as the radial gap gets larger. Furthermore, as a consequence of the different orientation and intensity of waves, at larger radial gap size the streamlines passing through the RR waves are deviated upward considerably.

On the other hand, increasing the radial gap size, the Left-Running (LR) expansion fan **C** must enlarge to both match the required expansion ratio and the flow direction of the streamlines coming from the bladed region. This then leads the expansion ratio across the radial gap to increase as the radial gap increases. An intermediate condition between the baseline case and the ΔR_5 case is instead reached for the ΔR_4 case, in which the angular extension of the two expansion fans is approximately symmetric, Fig. 5e. However, the combined effect of RR shock moving upstream and the LR expansion enlarging as the radial gap is increased leads the LR shock **D** and the reflected RR running shock to move closer while they travel downstream.

Another noticeable occurrence concerns the compression waves **E** which are originated from the curved rear suction side design. In fact, while at low radial gap size this set of weak compression waves is barely visible, at larger gap size they coalesce into a shock when they travel further downstream. Finally, the latter flow feature, together with larger wetted area and larger number of wakes mixing out in the radial gap as its size increases, can arguably explain the loss

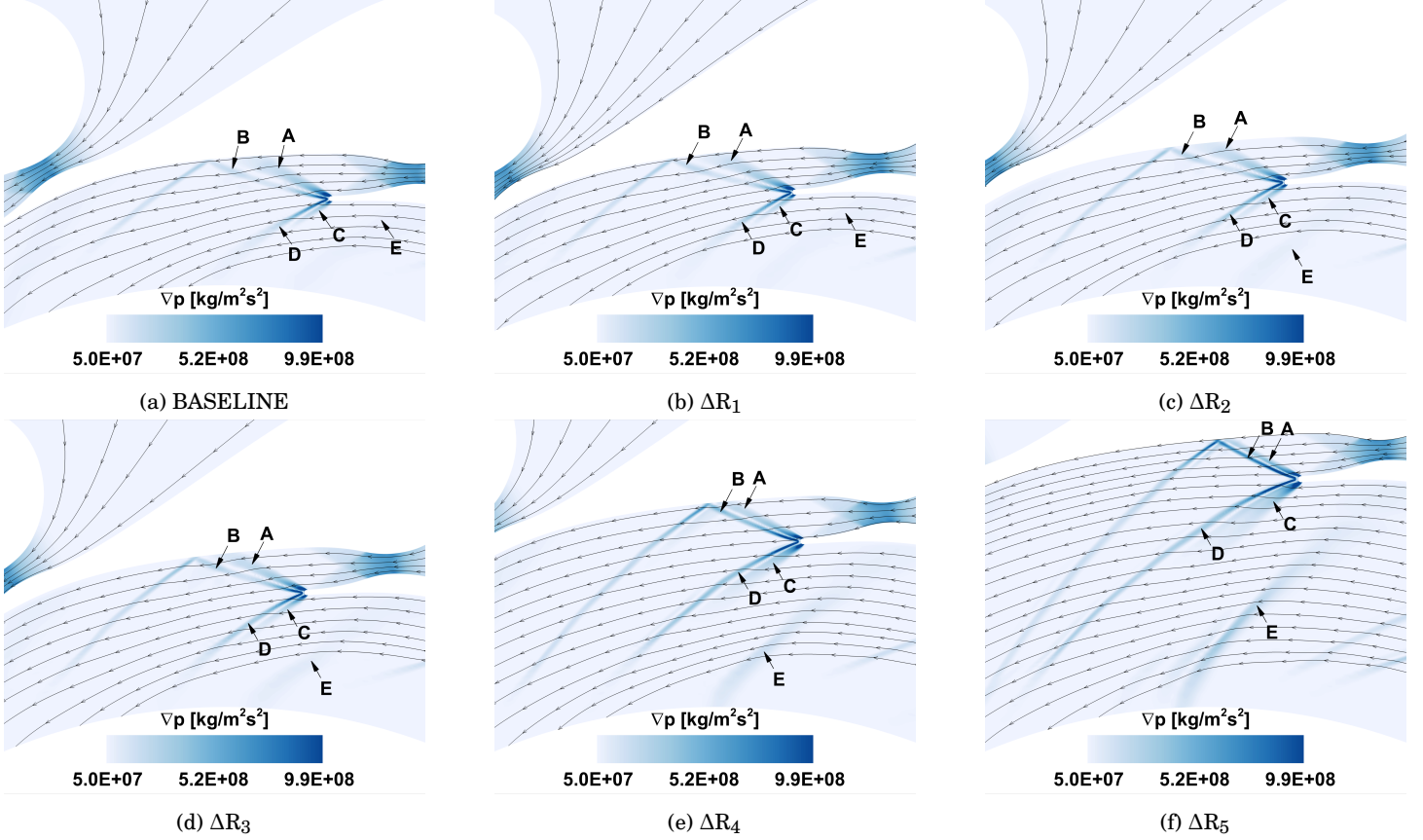


FIGURE 5: MID-SPAN PRESSURE GRADIENT CONTOURS: CLOSE-UP VIEW OF TE REGIONS.

increase occurring downstream of the stator TE as the radial gap increase, Fig. 3b.

The combination of the above-mentioned features also impacts the non-uniformity level of the pitch-wise distributions found at rotor inlet radius. The latter was computed for the absolute Mach number, Ma , absolute flow angle, α , and relative flow angle, β , pitch-wise distributions as in Eqn. 8 and the results are shown in Tab. 5. As one can notice, the variation of the three non-uniformity indexes against the radial gap size shows a non-monotone trend. Among the three investigated quantities, the relative flow angle non-uniformity is the most relevant one, since it directly links the non-uniformity to the incidence variability at rotor inlet. In this regard, the results presented in Tab. 5 suggest that large incidence variability is to be expected at rotor inlet, although the radial gap size could be regarded as a design variable to alleviate it.

$$\Delta Ma_2 = \frac{\int_0^{\theta_{pitch}} |Ma_2 - \overline{Ma_2}| d\theta}{\Delta\theta_{pitch}} \cdot \frac{100}{\overline{Ma_2}} \quad (8a)$$

$$\Delta\alpha_2 = \frac{\int_0^{\theta_{pitch}} |\alpha_2 - \overline{\alpha_2}| d\theta}{\Delta\theta_{pitch}} \cdot \frac{100}{\overline{\alpha_2}} \quad (8b)$$

$$\Delta\beta_2 = \frac{\int_0^{\theta_{pitch}} |\beta_2 - \overline{\beta_2}| d\theta}{\Delta\theta_{pitch}} \cdot \frac{100}{\overline{\beta_2}} \quad (8c)$$

In Fig. 8 the absolute flow angle development through the radial gap is shown as a function of the non-dimensional stream-wise location, for which the starting value 0 corresponds to the stator TE radius, R_1 , while the value 1 corresponds to the rotor LE radius, R_2 . While the overall flow angle deflection is approximately 1.5° for the baseline and ΔR_1 cases, larger flow angle changes occur from inlet to outlet of the gap at larger radial gap sizes.

Interestingly, the distributions start at different values of the flow angle –highlighting different values of the devi-

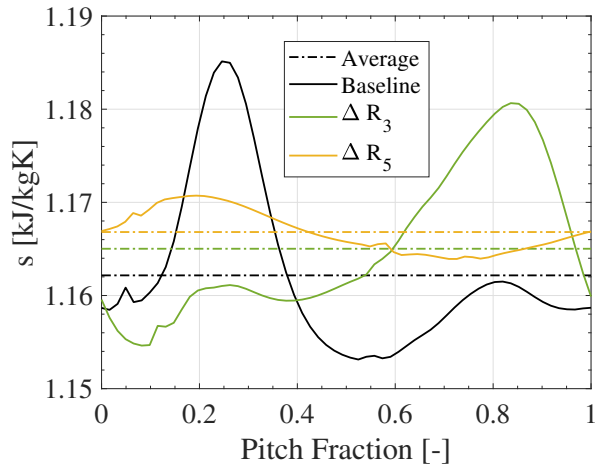


FIGURE 6: PITCH-WISE ENTROPY DISTRIBUTIONS AND AVERAGE VALUES AT ROTOR INLET RADIUS R_2 FOR BASELINE, ΔR_3 and ΔR_5 CASES

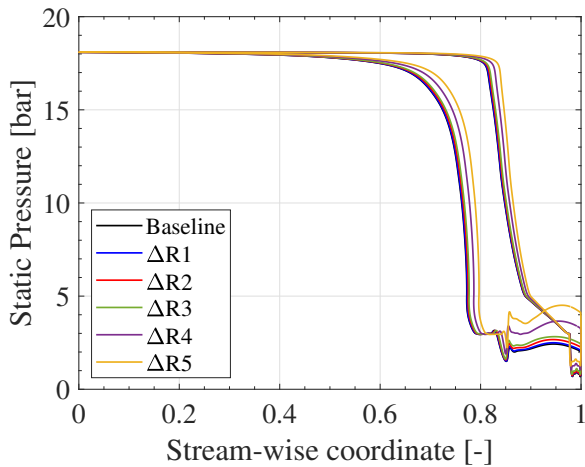


FIGURE 7: STATOR BLADE LOADING

ation angle— with an overall scatter of 4° . Furthermore, at the stator TE radius R_1 (0 radial gap stream-wise location) the flow becomes more and more tangential as the radial gap size increases. This observation can be easily explained with reference to the TE flow pattern change visible in the pressure gradient contour, Fig. 5a-5f. Particularly, one should consider that the RR expansion fan **A** turns the flow counter-clockwise, e.g., more radially, whereas the RR shock **B** turns the flow clockwise, e.g., more tangentially. Increasing the radial gap the RR expansion fan shrinks and the RR shock gets stronger. Therefore, the counter-clockwise turning is weakened and the clockwise turning is strengthened, with

TABLE 5: PITCH-WISE NON-UNIFORMITY LEVELS AT ROTOR INLET

	Baseline	ΔR_1	ΔR_2	ΔR_3	ΔR_4	ΔR_5
ΔMa_2	5.40	4.94	2.33	3.78	4.42	4.03
$\Delta \alpha_2$	3.92	3.78	3.33	3.08	2.95	2.99
$\Delta \beta_2$	36.17	33.92	17.78	26.10	31.37	37.76

net effect of producing a flow at R_1 surface more tangentially oriented. Additionally, the different flow angle values at the stator TE mitigate the flow angle difference at the rotor LE.

Stage Analysis

To perform the stage analysis and assess the impact of a radial gap change on the overall stage performance, two different numerical approaches have been used, i.e., steady-state RANS and unsteady-RANS calculations. The reflective nature of the mixing-plane implemented in the flow solver adopted throughout the work, together with the very high Mach number at stator discharge, which characterize the selected test case, and the tight radial gap have made impossible to the authors to avoid the presence of some spurious wave reflections originated from the mixing-plane in *Baseline* and ΔR_1 cases. These reflections may alter the flow field locally, making the reliability of mixing-plane simulation results somewhat doubtful. This reason pushed the authors to perform additional CFD calculations by means of unsteady RANS approach, which avoids the adoption of

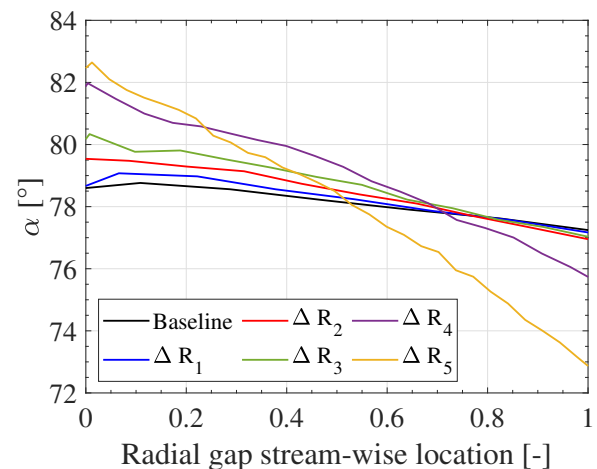


FIGURE 8: ABSOLUTE FLOW ANGLE IN THE RADIAL GAP. ANGLES MEASURED FROM RADIAL DIRECTION

a mixing-plane interface and, therefore, the spurious wave reflection, so providing un-biased data for RANS result validation. To make sure of covering the entire design space investigated with steady-state RANS, unsteady RANS have been performed on *Baseline*, ΔR_3 , ΔR_4 and ΔR_5 cases.

In Tab. 6 a comparison of RANS and time-average uRANS results is provided for some selected quantities of interest for the work, namely the total to total efficiency, η_{TT} , static pressure at the stator TE, p_1 , and static pressure at the stator-rotor interface, p_2 . As one can notice, quite good agreement is found between the two models concerning the total-total efficiency –with the relative difference below 1.5% in all cases– and the static pressure at stator TE, suggesting a negligible impact of above mentioned wave reflections. Concerning the static pressure at the stator-rotor interface, despite slightly larger discrepancy, RANS model still provides results which are in good agreement with the time-averaged uRANS results.

Figure 15 presents the comparison of the mid-span Mach number distributions of the RANS and time-average uRANS results for both baseline and ΔR_3 cases. As one can notice, exception made for the wave reflections at the mixing-plane of the baseline configuration, fairly similar distributions can be noticed, suggesting the reliability of RANS

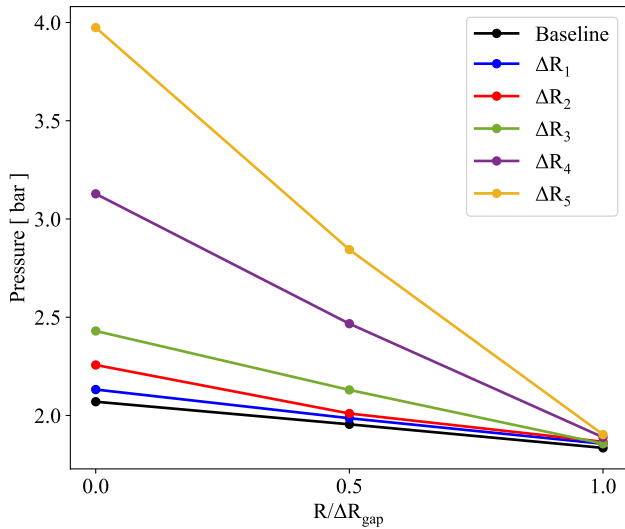


FIGURE 9: CIRCUMFERENTIAL-AVERAGED PRESSURE TREND IN THE RADIAL GAP. THE STATIC PRESSURE VARIATION WHICH IS OBSERVABLE AT THE END OF THE RADIAL GAP, I.E. AT THE INLET SECTION OF THE ROTOR ($R/\Delta R_{gap} = 1$), IS WITHIN 3.7 % OF THE BASELINE CASE'S ROTOR INLET STATIC PRESSURE.

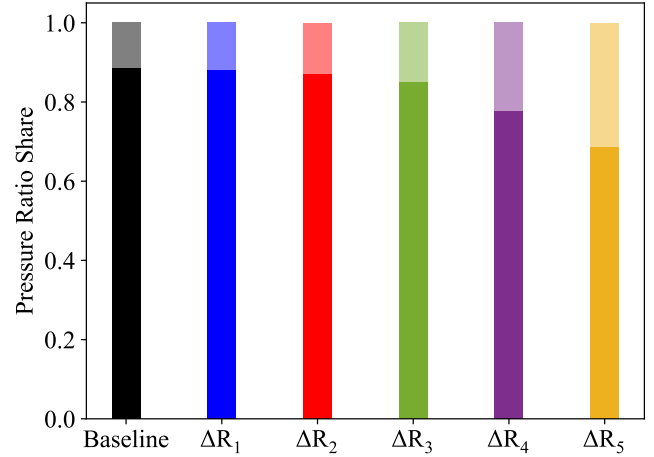


FIGURE 10: EXPANSION PROCESS SHARE IN THE STATIONARY PART OF THE MACHINE. SOLID COLOR BARS REPRESENT THE PART OF EXPANSION HAPPENING IN THE STATOR, WHILE THE TRANSPARENT ONES THAT HAPPENING IN THE RADIAL GAP.

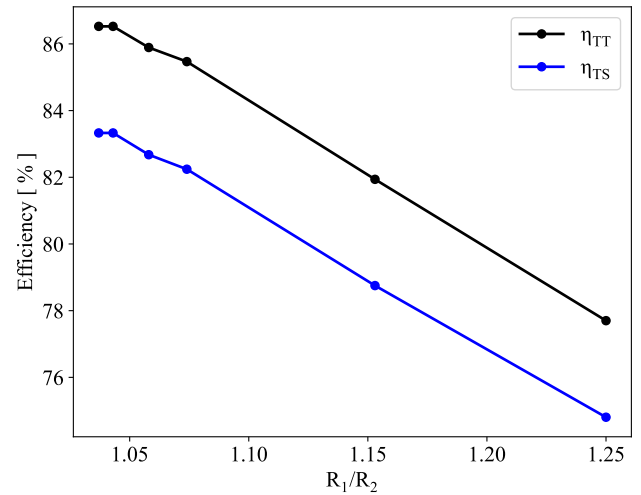


FIGURE 11: TOTAL-TOTAL AND TOTAL-STATIC STAGE EFFICIENCY

calculations. Finally, only minor differences can be seen in the size of the rotor suction side separation predicted by the steady and unsteady RANS calculations.

The comparison between RANS and uRANS computations made it possible to confidently draw conclusions based

TABLE 6: RANS AND uRANS RESULTS COMPARISON FOR BASELINE AND ΔR_3 CASES.

Case	η_{TT} (%)		p_1 (bar)		p_2 (bar)	
	RANS	uRANS	RANS	uRANS	RANS	uRANS
Baseline	86.5	85.3	2.08	2.07	1.83	1.78
ΔR_3	85.5	84.4	2.43	2.39	1.85	1.76
ΔR_4	81.9	81.7	3.13	3.09	1.89	1.79
ΔR_5	77.7	77.0	3.97	3.97	1.90	1.79

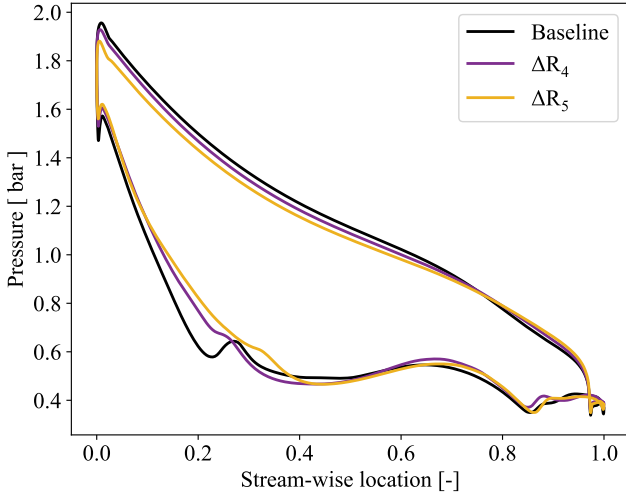


FIGURE 12: ROTOR BLADE LOADING FOR 3 RADIAL GAP SIZE

on the trends of integral quantities, such as efficiency and reaction degree, obtained through RANS simulations.

As for the stator simulations discussed in the previous section, the pressure at the inlet of the rotor cascade, p_2 , was found to be nearly constant among the different cases tested. Figure 9 shows the static pressure in the radial gap for all the geometries tested. Notably, the pressure at the rotor inlet section (point at $\Delta R = 100\%$ in the plot) corresponds relatively well throughout the set of stages investigated.

Figure 10 shows the pressure ratio redistribution anticipated in the section Stator Analysis. An observable trend of changing pressure ratio share between the stator and the radial gap suggests that, for increasing gaps size, the stator will operate in off-design conditions.

Figure 11 shows how the stage efficiency decreases for larger stator-rotor gaps. While the flow losses occurring in

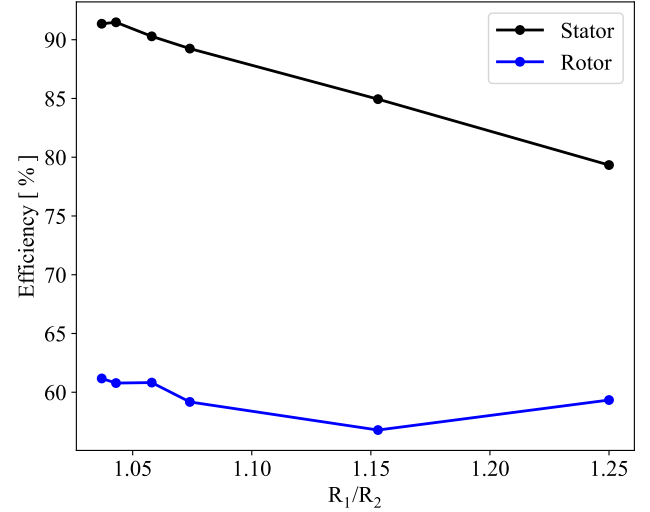


FIGURE 13: STATOR AND ROTOR EFFICIENCY AS FUNCTION OF RADIAL GAP SIZE

the stationary part increase – due to alterations in the shock pattern and to an increase in the flow-path length – the comparatively low efficiency of the rotating cascade from Fig. 13 would be explained by the large separation occurring on the SS of the rotor blades.

Figure 12 shows the rotor blade loading for three of the investigated cases. It can be derived that, despite minor differences in particular at the rotor LE due to slight incidence change, the rotor loading was unchanged throughout the different cases, which is in agreement with the relatively constant trend of rotor efficiency in Fig. 13, defined by Eqn. 9:

$$\eta_{R, Ise} = \frac{W_3^2}{W_{3, Ise}^2} \cdot 100 \quad (9)$$

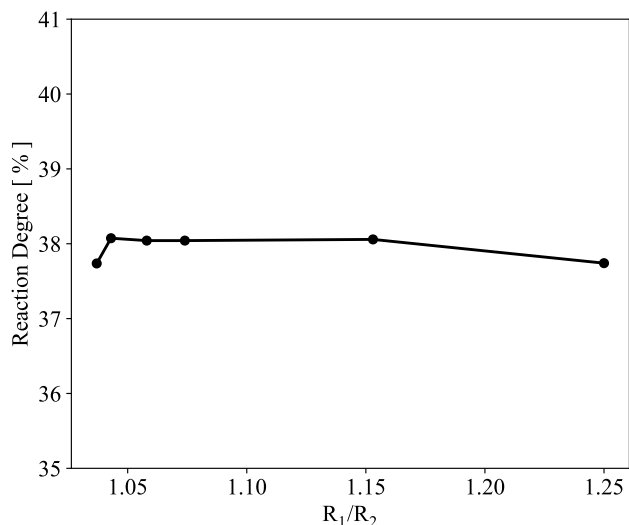


FIGURE 14: REACTION DEGREE VS RADIAL GAP VARIATION

On the other hand, the flow phenomenology in the stationary part of the machine described in the previous section similarly applies to the stage calculations shown in the present one. As a matter of fact, the stator efficiency from stage calculations shown in Fig. 13 compares relatively well with that from stator calculations of Fig. 3b.

While other authors (e.g., [6]) found an increase in actual reaction degree with the gap size, the present investigation shifts the attention to the isentropic reaction degree. Figure 14 shows, for the cases investigated here, that the isentropic reaction degree is relatively constant, which is a direct consequence of the minor effects the radial gap had on the rotor performance in this investigation. This observation finds direct applicability in the preliminary design of radial, centripetal supersonic turbine stages, suggesting that the choice of the reaction degree is independent of detailed design considerations.

CONCLUSIONS

In this work, the effect of the stator-rotor radial gap size for supersonic RIT stages has been examined. To this end, stators with varying outlet radius have been designed, so to provide a change in radial gap size.

Subsequently, isolated row and stage 3D CFD calculations have been carried out by means of RANS model, while as a higher fidelity tool, uRANS calculations have been used to assess the accuracy of stage results. In addition, an analytical quasi-1D gas-dynamic model, describing the effect of

the radial gap size on the ratio between the expansion ratio of the vanned part and that of the vaneless space, has been developed and verified numerically.

The isolated row calculations allowed the evaluation of the effect of the radial gap size on the expansion ratio occurring in the vaneless space, which increased by increasing the radial gap. This was accompanied by a substantial change in the trailing-edge flow pattern. In turn, the flow structure change was correlated with the loss increase occurring both in the vanned and vaneless regions as the radial gap increased. Furthermore, the impact of the radial gap on the wake profile found at the rotor inlet radius was assessed, along with the effect on the uniformity of the pitch-wise flow quantities at the rotor inlet. Results showed that, while the radial gap size has a strong impact on the circumferential flow distributions and wake profile at rotor inlet, its size could be used to mitigate the fluctuations of the rotor incidence angle.

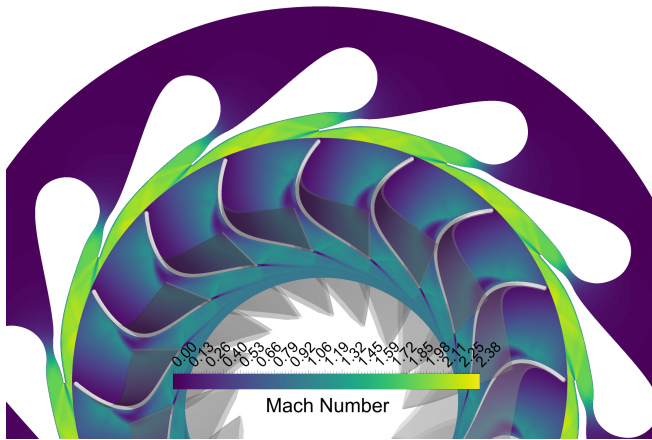
Results from stage simulations highlighted that the ratio of the expansion ratio between the vanned and the vaneless space was in a rather good agreement with the trend predicted by the analytical model. Therefore, isolated stator simulations are suited to investigate the effect of the radial gap on the vane and vaneless space fluid-dynamic performance. Moreover, the stator loss increase is clearly reflected into a non-negligible stage efficiency penalty, whose monotonic trend was further corroborated by the results of uRANS simulations. Besides, while the rotor blade loading and the reaction degree did not vary significantly between the different cases analysed, its isentropic efficiency was largely impacted by the change of the upstream conditions as the radial gap is varied.

Eventually, the trends of loss and expansion ratio observed suggest that decreasing the target Mach number at the outlet of the diverging section of the supersonic stator might improve the stage efficiency as the radial gap is increased. For this reason, future work will be targeted to investigating this aspect and to further expand the design space.

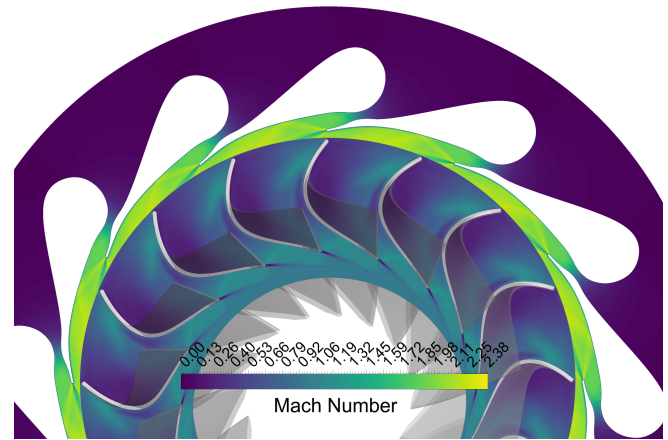
ACKNOWLEDGMENT

This research was supported by the Dutch Technology Foundation TTW, Applied Science Division of NWO, the Technology Program of the Ministry of Economic Affairs, and by the project partners (Grant No. 17906).

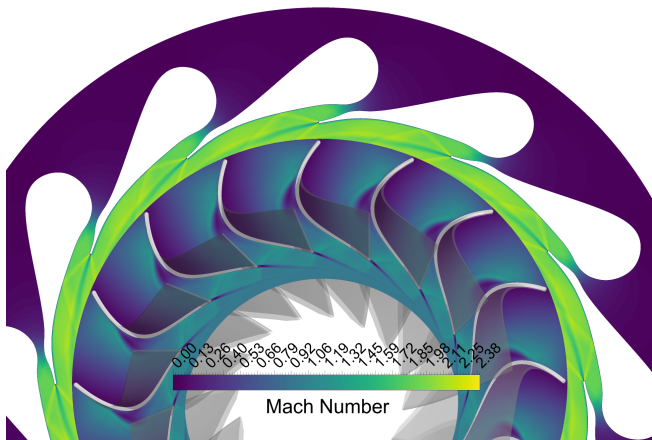
The authors want to thank their colleagues Frank and Steve, of TU Delft's work-shop DEMO, for their precious advise regarding manufacturing aspects.



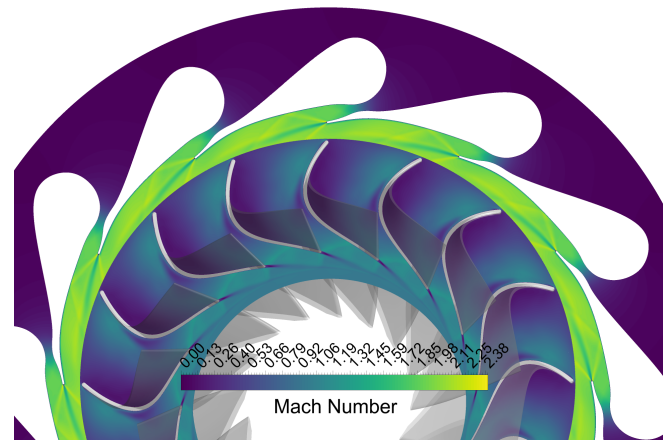
(a) BASELINE - RANS



(b) BASELINE - TIME-AVERAGE URANS



(c) ΔR_3 - RANS



(d) ΔR_3 - TIME-AVERAGE URANS

FIGURE 15: COMPARISON OF MID-SPAN MACH NUMBER DISTRIBUTIONS: RANS VS TIME-AVERAGE URANS RESULTS.

REFERENCES

- [1] , 2020. Supertruck ii 2020 program update. from Dieselnet website, July. Last accessed on Dec. 22, 2021—See <https://dieselnet.com/news/2020/07supertruck.php>.
- [2] Astolfi, M., Baresi, M., van Buijtenen, J., Colonna, P., David, G., Beul, L. D., Garofalo, F., Ruggiero, M., Sanchez, D., Wieland, C., and Zampieri, G., 2021. Thermal Energy Harvesting - the Path to Tapping into a Large CO₂-free European Power Source. White paper report, KCORC - TEHAG. Last accessed on Dec 22, 2021—See <https://www.kcorc.org/en/committees/thermal-energy-harvesting-advocacy-group/>.
- [3] P. Colonna, M. P., and Vos., R. Arena: Airborne energy harvesting for aircraft. Nederlandse Organisatie voor Wetenschappelijk Onderzoek-domein Toegepaste en Technische Wetenschappen: Open Technology Programme, (Project 17906), 2020-2024.
- [4] De Servi, C. M., Burigana, M., Pini, M., and Colonna, P., 2019. “Design method and performance prediction for radial-inflow turbines of high-temperature mini-organic rankine cycle power systems”. *Journal of Engineering for Gas Turbines and Power*, **141**.
- [5] Tunakov, A., 1961. Effect of the radial clearance on the operation of a centripetal gas turbine. Tech. rep., FOREIGN TECHNOLOGY DIV WRIGHT-PATTERSON AFB OHIO.
- [6] Watanabe, I., Ariga, I., and Mashimo, T., 1971. “Effect of dimensional parameters of impellers on performance characteristics of a radial-inflow turbine”. *Journal of Engineering for Gas Turbines and Power*, **93**, 1, pp. 81–

- 102.
- [7] Khalil, I. M., Tabakoff, W., and Hamed, A., 1976. “Losses in radial inflow turbines”. *Journal of Fluids Engineering, Transactions of the ASME*, **98**, 9, pp. 364–371.
- [8] Simpson, A. T., Spence, S. W., and Watterson, J. K., 2013. “Numerical and experimental study of the performance effects of varying vaneless space and vane solidity in radial turbine stators”. *Journal of Turbomachinery*, **135**, 3.
- [9] Wheeler, A. P. S., and Ong, J., 2013. “The role of dense gas dynamics on organic rankine cycle turbine performance”. *Journal of Engineering for Gas Turbines and Power*, **135**.
- [10] Anand, N., Vitale, S., Pini, M., Otero, G. J., and Pecnik, R., 2018. “Design methodology for supersonic radial vanes operating in nonideal flow conditions”. *Journal of Engineering for Gas Turbines and Power*, **141**(2), nov.
- [11] Thompson, P. A., 1971. “A fundamental derivative in gasdynamics”. *The Physics of Fluids*, **14**(9), pp. 1843–1849.
- [12] Colonna, P., and Guardone, A., 2006. “Molecular interpretation of nonclassical gas dynamics of dense vapors under the van der waals model”. *Physics of Fluids*, **18**(5), may, p. 056101.
- [13] Baumgärtner, D., Otter, J. J., and Wheeler, A. P. S., 2020. “The effect of isentropic exponent on transonic turbine performance”. *Journal of Turbomachinery*, **142**.
- [14] Giuffrè, A., and Pini, M., 2021. “Design guidelines for axial turbines operating with non-ideal compressible flows”. *Journal of Engineering for Gas Turbines and Power*, **143**(1), p. 011004.
- [15] Galiana, F. J. D., Wheeler, A. P., and Ong, J., 2016. “A study of trailing-edge losses in organic rankine cycle turbines”. *Journal of Turbomachinery*, **138**(12), jun.
- [16] Galiana, F. D., Wheeler, A., Ong, J., and de M Ventura, C., 2017. “The effect of dense gas dynamics on loss in ORC transonic turbines”. *Journal of Physics: Conference Series*, **821**, mar, p. 012021.
- [17] Baumgärtner, D., Otter, J. J., and Wheeler, A. P., 2020. “The effect of isentropic exponent on supersonic turbine wakes”. In *International Seminar on Non-Ideal Compressible-Fluid Dynamics for Propulsion & Power*, Springer, pp. 153–161.
- [18] Pini, M., Persico, G., Pasquale, D., and Rebay, S., 2014. “Adjoint method for shape optimization in real-gas flow applications”. *Journal of Engineering for Gas Turbines and Power*, **137**(3), oct.
- [19] Cappiello, A., and Tuccillo, R., 2021. “Design parameter influence on losses and downstream flow field uniformity in supersonic ORC radial-inflow turbine stators”. *International Journal of Turbomachinery, Propulsion and Power*, **6**(3), sep, p. 38.
- [20] Rinaldi, E., Pecnik, R., and Colonna, P., 2016. “Unsteady operation of a highly supersonic organic rankine cycle turbine”. *Journal of Turbomachinery*, **138**(12), jul.
- [21] Cappiello, A., and Tuccillo, R., 2021. “Influence of supersonic nozzle design parameters on the unsteady stator-rotor interaction in radial-inflow turbines for organic rankine cycles”. In *Turbo Expo: Power for Land, Sea, and Air*, American Society of Mechanical Engineers.
- [22] Anand, N., Colonna, P., and Pini, M., 2020. “Design guidelines for supersonic stators operating with fluids made of complex molecules”. *Energy*, **203**, jul, p. 117698.